Inorganic Chemistry

pubs.acs.org/IC Article

# Facile Ferroelectric Phase Transition Driven by Si Doping in $HfO_2$

Hyemi Yang,[†] Kunwoo Park,[†] Hyun-Jae Lee, Jinhyeong Jo, Hayoung Park, Noejung Park, Jungwon Park,* and Jun Hee Lee*

Cite This: *Inorg. Chem.* 2020, 59, 5993−5999 Read Online

ACCESS | Metrics & More | Article Recommendations | Supporting Information

**ABSTRACT:** The recently discovered ferroelectricity in thin-film orthorhombic $HfO_2$, which can be directly integrated into complementary metal−oxide semiconductor technology, has become an important research target. However, the use of orthorhombic $HfO_2$ in practical devices has been limited by undesirable mixing with the monoclinic phase, which is nonpolar and thus degrades the ferroelectric properties. Here, we demonstrate that a Si dopant significantly stabilizes the ferroelectric phase because of its unique bonding characteristics, particularly its intrinsic tendency to form strong covalent bonds with O, thereby weakening the phase boundary to stabilize the ferroelectric orthorhombic phase over the nonpolar monoclinic phase, relatively. On the basis of our theoretical predictions, we conducted transmission electron microscopy measurements and confirmed that Si substitution doping indeed induced monoclinic structural components into the orthorhombic phase, which is a strong indication of the weakened phase boundary and subsequent facilitation of the ferroelectric transition. This work thus provides an atomic-scale picture for understanding the unique role of Si in promoting the ferroelectric phase and the dopant dependence on the wake-up effect in $HfO_2$, offering a substantial advancement toward integrating ferroelectrics into practical devices.

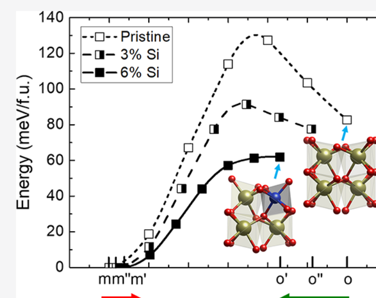


## 1. INTRODUCTION

$HfO_2$ is of practical interest because it can be directly integrated into current complementary metal−oxide semiconductor technology. The various structural phases of $HfO_2$, such as the monoclinic (m-) and orthorhombic (o-) phases, compete strongly with one another, and selecting the appropriate structural phase for a given application is very important. For example, the tetragonal phase, with a large dielectric constant,[1,2] is usually used for high-*k* gate dielectric devices, whereas the o-phase is preferable for ferroelectric field-effect transistors or capacitors,[3] and the amorphous or m-phases, containing a conductive filament under $1.5 \times 10^{21}$ $cm^{-3}$ of O vacancy concentration, are also expected to be used in memory devices.[4] Since the ferroelectric $HfO_2$ was discovered in 2011, various efforts have been undertaken to stabilize the ferroelectric o-phase, with techniques ranging from chemical (doping[5,6] and electrode materials[7]) to physical (surface or grain boundary effects[8] and stress[7,9]) and technical (capping electrode[4,10−14] and formation temperature[8,15]).

However, even with these efforts, several factors continue to hinder the commercial application of $HfO_2$. Ferroelectric o-phase films are inevitably mixed with the undesirable nonpolar phases (especially with the ground-state m-phase),[16−18] which degrade the ferroelectric properties. In addition, the so-called "wake-up" phenomenon,[19] in which polarization continues to increase with electric-field cycling even after fabrication, limits the stability of practical devices. To handle the former problems, various dopants have been tried to date, both experimentally (Ba,[6] Y,[5,6,18,20] Al,[5,6,21] Er,[6,20] Nd,[6,20] Sm,[6,20] Sr,[5] La,[5,6,20,21] Si,[5,21] Gd,[5,21] Sc,[18] Ge,[18] and Zr[18]) and theoretically (Si,[22−25] C,[23] Ge,[23] Ti,[23] Sn,[23] Zr,[23] Ce,[23] Sr,[24−27] La,[25−28] Y,[26,28] Al,[28] and Ba[26]) to figure out the obvious ferroelectricity and origin of the ferroelectric properties of $HfO_2$ with a doping effect. Also, the latter problems were studied using various dopants.[21,29−31] Even though many doping studies have been done revealing a dopant effect on the ferroelectricity of $HfO_2$, analyses of various dopants from an atomic perspective are still needed to understand the origin of promoting the ferroelectricity in $HfO_2$ and to reduce the deleterious effects that currently limit its application.

In this study, we carefully examined the relative stabilities of the m- and o-phases in $HfO_2$ with various dopants and subsequent phase transition from the m-phase to o-phase after doping. We thereby discovered that Si and La dopants produced remarkable stabilization of the desirable o-phase. In particular, the Si dopant displayed the unique characteristic of forming strong covalent bonds with O, which plays an exclusive role in enhancing structural isosymmetries between the m- and o-phases and thus facilitates the transition from the m-phase to o-phase. Si doping was thus expected to induce anisotropic structural changes even in the o-phase. This

**Received:** December 31, 2019
**Published:** April 21, 2020

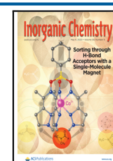

Downloaded via ULSAN NATL INST SCIENCE AND TECHLGY on November 20, 2023 at 04:45:35 (UTC).
See https://pubs.acs.org/sharingguidelines for options on how to legitimately share published articles.

ACS Publications © 2020 American Chemical Society



https://dx.doi.org/10.1021/acs.inorgchem.9b03785
*Inorg. Chem.* 2020, 59, 5993−5999

prediction was motivated by scanning transmission electron microscopy (STEM) analyses that showed strong local shear strain (m-phase characteristics) in the o-phase. This research can thus inform a strategy for stabilizing the ferroelectric o-phase with respect to the ground-state m-phase and effectively tuning the undesirable "wake-up" effect.

## 2. EXPERIMENTAL SECTION

**Sample Preparation.** The TiN/Si:$HfO_2$/TiN metal−ferroelectric−metal (MFM) capacitors were fabricated on a Si(001) substrate. 12-nm-thick TiN bottom and top electrodes were deposited by chemical vapor deposition, and an 8-nm-thick 4.2% Si-doped $HfO_2$ thin film was deposited by atomic layer deposition of tetrakis-(dimethylamido)hafnium, tetrakis(dimethylamino)silane, and ozone. The stacks were passed through an 800 °C annealing process in ambient $N_2$ for 1 s.

**STEM Measurements.** For cross-sectional STEM observation, the MFM stack was fabricated into a thin lamella using a focused ion beam (FEI Helios). The lamella was observed with an aberration-corrected Titan G2 microscope (60−300 kV) operated at 200 kV. The convergence and high-angle annular dark-field detector collection semiangles were 26 and 36 mrad, respectively.

## 3. RESULTS AND DISCUSSION

To investigate the effects of doping on the o-phase ($Pca2_1$) stability relative to that on the m-phase ($P2_1/c$), we calculated the energy difference between the m- and o-phases of $HfO_2$ in the presence of dopants. According to a 2017 report,[27] charge-compensated defects of Sr(Hf)V(O) showed that a nonferroelectric tetragonal ($P4_2/nmc$) phase was energetically preferred to the o-phase, whereas charge-uncompensated defects of Sr(Hf), in O-rich conditions, reduced the energy difference between the m- and o-phases, stabilizing the ferroelectric o-phase relative to the m-phase. We found a similar trend in the energy difference between the m- and o-phases. Dopants were substituted for Hf [D(Hf) defects] in 2 × 2 × 2 supercells containing 96 atoms under charge-uncompensated O-rich conditions.[8,23] Simulations are based on a bulk structure, especially for small atomic-scale conditions, which does not reflect the grain size effect because of realistic limitations on the computational size, so they only give insight into film samples. Figure 1a shows the energy differences between the ground-state m-phase and ferroelectric o-phase for various dopants. The energy difference between the two phases was defined as in eq 1:

$$\Delta E\ (\text{meV f. u.}^{-1}) = E(\text{O}) - E(\text{M}) \tag{1}$$

where O and M denote the o- and m-phases, respectively. We determined that the larger the difference in the ionic radii of the dopants compared to Hf, the greater the relative stability of the o-phase. Si and La had significant effects, consistent with experimental results reported in 2017.[18] Also, according to previous works,[25] in the La-doped $HfO_2$ case, the O vacancy can decrease the energy of the o-phase below our calculation result and, thus, increase the structural stability of the o-phase.

To determine the extent of o-phase stability driven by Si and La, structures of doped m- and o-phases were decomposed into phonon modes with respect to the high-symmetry cubic (c-) phase, $Fm\bar{3}m$, as reported in 2014.[32] We discovered that Si doping causes structural deformation that increases the similarity between the m- and o-phases, in contrast to La doping (for more information, see Figures S1−S3).

Parts b and c of Figure 1 show the calculated phonon displacements for the m- and o-phases of $HfO_2$ doped with 0%,

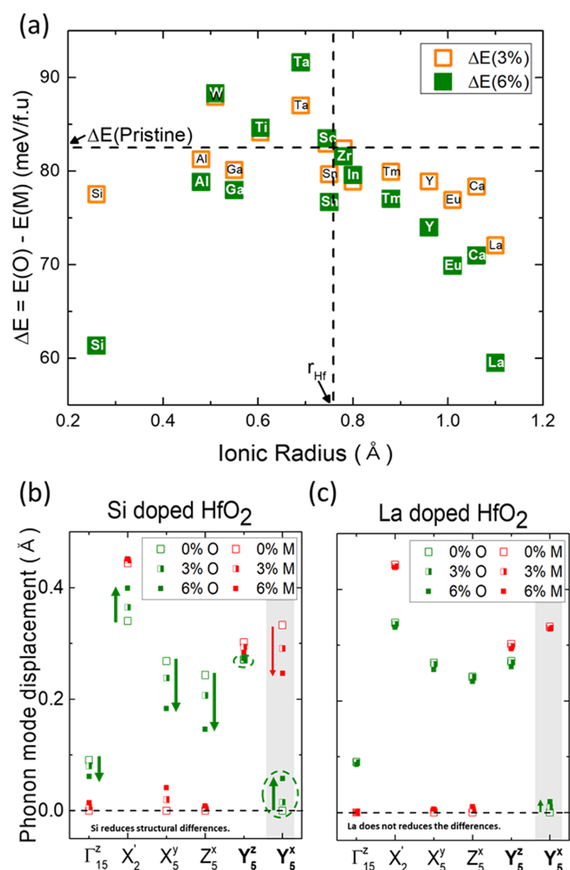


**Figure 1.** (a) Relative total energies of the o-phase ($Pca2_1$) with respect to the m-phase ($P2_1/c$) of $HfO_2$ with dopant contents of 0% (dashed horizontal line), 3.125% (in short 3%, orange), and 6.25% (in short 6%, green) against the ionic radius. Phonon-mode analysis for the m- and o-phases with (b) Si and (c) La with the above doping concentrations. The m- and o-phases are presented in red and green, respectively, and the open, half-filled, and fully filled squares denote 0%, 3.125%, and 6.25% doping concentrations, respectively. The shaded gray area indicates a newly formed mode in the doped o-phase compared to the pristine o-phase. Red and green arrows indicate increasing and decreasing tendencies of m- and o-phase phonon-mode displacements from 0% to 6.25%.

3.125% (denoted as 3% in the figure), and 6.25% (denoted as 6% in the figure) Si and La. In the case of Si, as the doping concentration increased, the displacements of phonon modes exclusive to the o-phase (Γ, $X_5^y$, and $Z_5^x$) decreased toward the m-phase, which does not exhibit those modes, whereas the displacements of other modes ($X_2'$, $Y_5^z$, and $Y_5^x$) tended to increase toward the m-phase. Most notably, $Y_5^x$, which was originally exclusive to the m-phase, began to emerge in the o-phase and decrease in the m-phase. Therefore, all of the phonon displacements previously associated with the o-phase or m-phase became similar to each other, significantly enhancing structural isosymmetries between the phases. In addition, structural deformation in the o-phase was more prominent than that in the m-phase, as shown in Figure 1b (see also Figure S8). Because Si doping is known to increase the fraction of the o-phase and subsequent polarization in thin films,[21] we suggest that Si is a strong o-phase stabilizer that weakened the boundary between the o- and m-phases.

In contrast, in the case of La-doped $HfO_2$, shown in Figure 1c, the phonon displacement of each mode barely changed even after the doping concentration increased by up to 6%,

showing a volume change by 2.6–2.7% only. Therefore, structural deformation was considerably smaller compared to that of Si-doped $HfO_2$, even with the high doping concentration. Therefore, heavy La doping can be expected to produce no significant structural distortion of host $HfO_2$. In fact, La doping has been reported up to ∼25% experimentally.[21]

To investigate the potentially large structural deformations induced by Si doping, we analyzed local bonding characteristics near the Si dopant by density functional theory (DFT) calculations and found that Si–O bonding forms a unique structure in o-$HfO_2$. The coordination number of Hf–O bonding in undoped o-$HfO_2$ is 7,[23] and for Si- and La-doped o-$HfO_2$, the coordination number of Si–O bonding is 6 and that of La–O is 7, as shown in Figure 2a,b. The original chemical environment of Hf–O in undoped o-$HfO_2$ would change with Si doping but not with La doping. Si doping causes structural deformation that rearranges the surrounding O atoms to form local octahedral structures with six bonds with the surrounding O atoms. Si-doped tetragonal $HfO_2$ was previously reported to stabilize because Si formed $SiO_2$ (quartz)-like structures locally.[22] In the same manner, we suggest that Si-doped o-$HfO_2$ contains local structures consistent with the stishovite (rutile) structure of silicon oxide ($SiO_2$) in nature, as shown in Figure 2c,d. The stishovite $SiO_2$ structure has similar internal atomic positions and a tilted lattice, in which a $\beta$ angle of not 90° exists between the $a$ and $c$ axes, as in Figure 2d, and these positions are similar to those of the ground state of $HfO_2$ (m-phase $HfO_2$), as shown in Figure S5. Therefore, the structural similarity between stishovite and undoped m-$HfO_2$ is considered to contribute to the dramatic stabilization of the o-phase with Si doping (Figure S5).

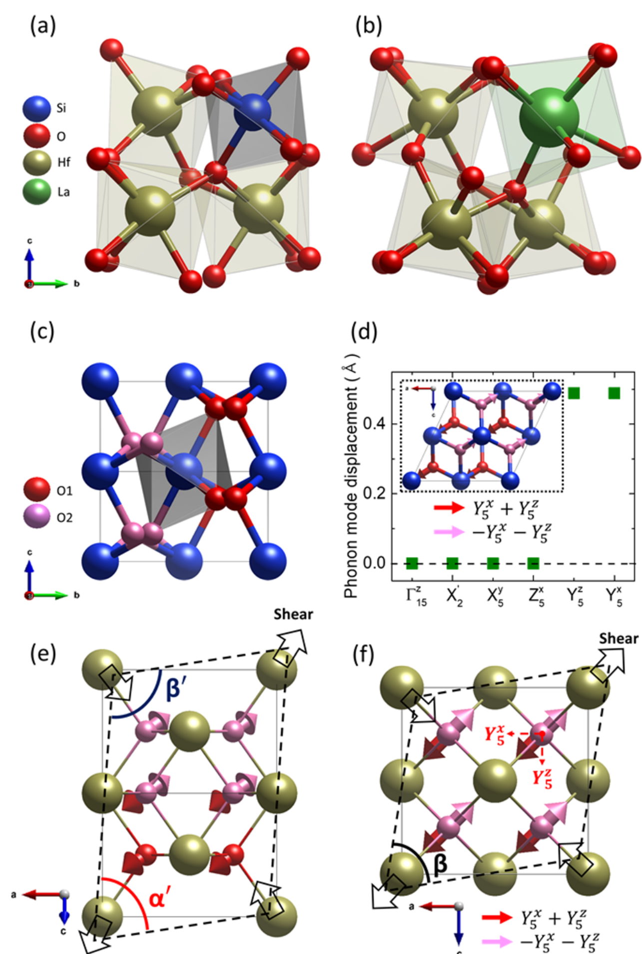


Figure 2. Structural analyses of (a) Si-doped and (b) La-doped o-$HfO_2$. (c and d) Stishovite structure ($SiO_2$) and (e and f) graphical illustration of the shear strain direction in $HfO_2$. Si, O, Hf, and La atoms are shown in blue, red/pink, olive, and green, respectively. In parts c–f, O1 and O2 are marked in red and pink to distinguish different O layers. (a–c) Translucent polyhedral structures show the bonding environment between the O and central atoms. (d–f) The $Y_5^z$ + $Y_5^x$ displacement directions in stishovite (inset) and $HfO_2$ are denoted by pink and red arrows, respectively. (e and f) Dashed lines and open arrows show the expected deformation of the Hf framework and shear strain directions induced by combined $Y_5^z$ + $Y_5^x$ modes.

We further performed phonon-mode analysis of the stishovite structure and confirmed that, as shown in Figure 2d, only $Y_5^z$ and $Y_5^x$ survived among the six phonon modes in Figure 1b,c. Among the modes, $Y_5^x$ was originally exclusive to the m-phase. As the Si doping concentration increased, displacement of the $Y_5^x$ mode emerged even in the o-phase, as shown in Figure 1b. The originally present $Y_5^z$ and newly emerged $Y_5^x$ formed a local stishovite structure in the Si-doped o-phase, leading to structural similarity to the ground state (m-phase) because of the monoclinic component of the stishovite structure. Furthermore, the direction of O displacement driven by the $Y_5^z$ + $Y_5^x$ modes, as shown in Figure 2e,f, coincided with the direction of O displacement in the stishovite structure shown in Figure 2d (inset): half of the O atoms moved diagonally on the $ac$ plane ($a$ + $c$), and the other half moved in the opposite direction. The O displacement of $Y_5^z$ + $Y_5^x$ driven by Si doping was expected to push out the Hf framework, tilting the $\beta$ angle of the lattice as in the m-phase and resulting in the expected structural deformations indicated by the dashed line in Figure 2e,f. In summary, we found that Si doping induced the original bonding characteristics of the stishovite structure even in the o-phase $HfO_2$. This unique local structure induced by Si created m-phase structural components in the o-phase, resulting in a weakening of the phase boundary between the o- and m-phases that supported the stability of the former. In contrast to the Si case, La did not induce significant structural deformation, as shown in the phonon-mode analysis in Figure 1c. La was expected to support o-phase stabilization mechanisms different from those of Si. Previous studies suggested that the ionic radius or electronegativity could be a significant factor in o-phase stabilization.[26] However, we still do not fully understand the o-stabilizing role enacted by La doping, although we found that hole doping, by such as $La^{3+}$, $Ca^{2+}$, or $Y^{3+}$, could be another o-phase stabilizer (Figure S7). For example, electron-doping cases such as $W^{6+}$, with $Ta^{5+}$ as a counterpart, are shown to destabilize the o-phase, as in Figure 1a. Therefore, we suggest that a neutral Si dopant is a special o-phase stabilizer that causes structural deformation and weakens the phase boundary.

On the basis of these predictions from our DFT calculations, we compared simulated transmission electron microscopy (TEM) images of 0%, 3.125%, and 6.25% Si-doped $HfO_2$ DFT models with the STEM images of 4.2% Si-doped $HfO_2$ capacitors experimentally obtained with aberration-corrected STEM. The consistency between the simulated and experimental data confirmed that m-phase components such as tilted angles ($\alpha'$ and $\beta'$) and atomic distances (⟨111⟩ and ⟨−111⟩), which are induced by Si doping, were involved in the


https://dx.doi.org/10.1021/acs.inorgchem.9b03785
Inorg. Chem. 2020, 59, 5993−5999

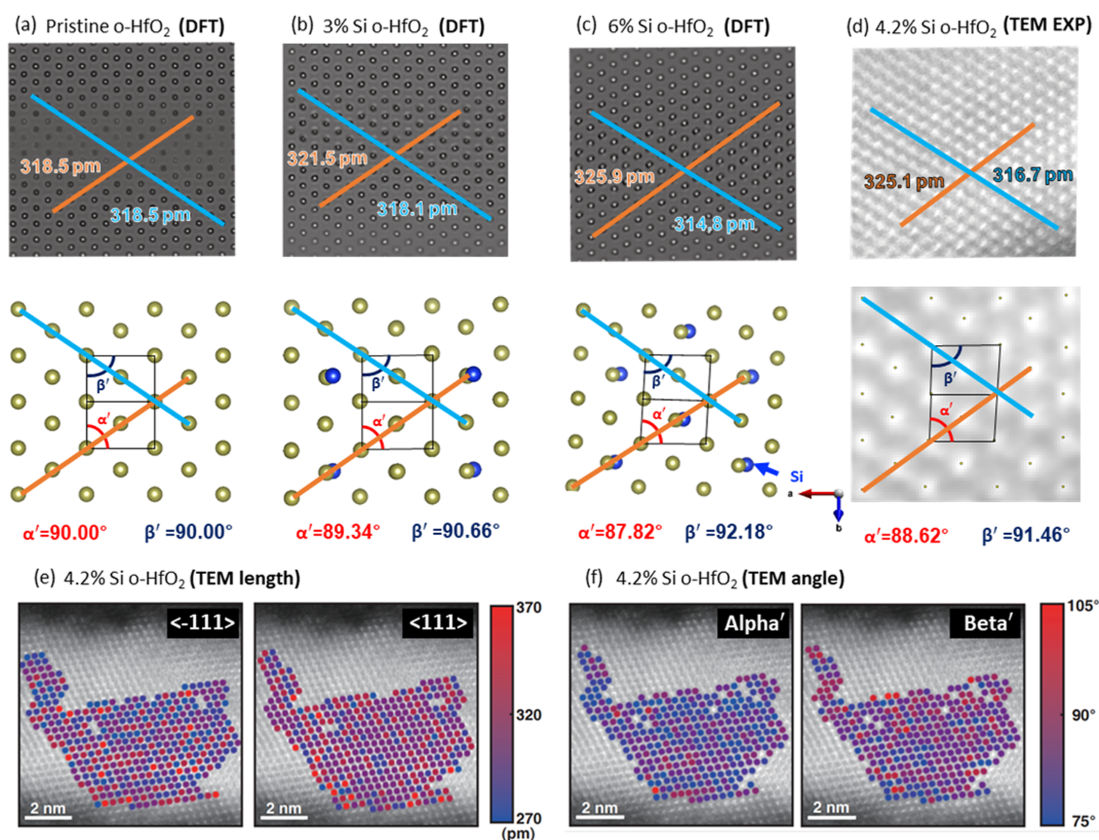


**Figure 3.** STEM images with $[0\bar{1}1]$ zone axes of Si-doped o-$HfO_2$: (a−c) simulated STEM images of 0%, 3.125%, and 6.25% doping concentrations; (d−f) experimental STEM images of 4.2% doping concentration. To distinguish from the crystallographic angle notation, the angles are denoted as $\alpha'$ and $\beta'$.

o-phase and weakened the boundary between the m- and o-phases. The average atomic distance was measured based on the intensity profiles in the (S)TEM images for each doping concentration with $[0\bar{1}1]$ zone axes. The simulated TEM images of the o-phase $HfO_2$ structure with different Si doping concentrations are shown in Figure 3a−c. In the simulated TEM image of undoped o-$HfO_2$, the interatomic distances along the orange line $\langle 111 \rangle$ and blue line $\langle -111 \rangle$ were identical, at 318.5 pm. The measured $\alpha'$ and $\beta'$ angles were 90°. These results indicated that there was no structural distortion with zero shear strain in the crystal structure of undoped o-$HfO_2$ (Figure 3a). However, with the 3.125% doping concentration, the atomic distances along the orange and blue lines were 321.5 and 318.1 pm, representing an increase of 0.94% and a decrease of 0.12%, respectively, compared to the undoped case (Figure 3b). This tendency was more significant with the 6.25% doping concentration. The measured atomic distance along the orange line increased by 2.32% to 325.9 pm, and that along the blue line decreased by 1.16% to 314.8 pm (Figure 3c). The length differences between the two lattice directions included structural distortion and were proportional to the Si doping concentration. These observations were also consistent with changes in the $\alpha'$ and $\beta'$ angles in the simulated TEM images for different doping levels. Compared to the undoped o-$HfO_2$, the $\alpha'$ values measured with the 3.125% and 6.25% concentrations were reduced by 0.66° and 2.18°, corresponding to shear strains of 0.01634 and 0.05406, respectively (Figure 3a−c). The interatomic distances and $\alpha'$ and $\beta'$ angles measured in the STEM image of experimentally prepared 4.2% Si-doped $HfO_2$ further confirmed that Si doping caused structural distortion (Figure 3d). The average atomic distances measured in the STEM image were 325.1 pm (an increase of 2.07%) and 316.7 pm (a decrease of 0.56%) along the orange and blue lines, respectively. The average $\alpha'$ value was reduced by 1.38°, indicating a shear strain of 0.03406. As shown in Figure 3e, the interatomic distance along the $\langle 111 \rangle$ plane was generally longer than that along the $\langle -111 \rangle$ plane. The distribution of $\alpha'$ angles was likewise lower than 90°, whereas the distribution of $\beta'$ angles was centered at over 90° (Figure 3f). Overall, the shear strains estimated based on the $\alpha'$ angle measured from (S)TEM images of different doping levels showed a linear relationship. The direction of structural distortion induced by Si was the same as the original direction of distortion in the m-phase structure (Figures S8−S11), and the tendency of the change of the two phonon displacements with increasing doping concentrations followed the m-phase, again confirming the stabilizing role of Si in producing monoclinic character in the o-phase. In conclusion, we confirmed the overall structural distortion caused by Si doping by using a combination of high-resolution STEM imaging of an experimentally prepared film and TEM simulations assisted by DFT calculations.

Motivated by the structural similarities enhanced by the doping, we calculated the corresponding activation energies between the m- and o-phases. The most favorable phase-transition route from the m-phase to the o-phase was found by matching the direction of the $X_2'$ and $Y_5^z$ phonon modes, which are commonly present in both the m- and o-phases. The structural pathways of the transition between the m- and o-phases ($x$ axis in Figure 4) modified by doping (L′ in Figure



https://dx.doi.org/10.1021/acs.inorgchem.9b03785
Inorg. Chem. 2020, 59, 5993−5999

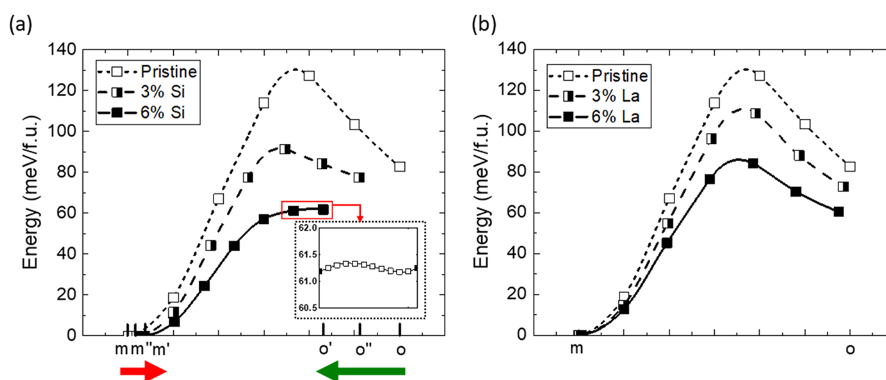


**Figure 4.** Phase-transition energy (from the m-phase to the o-phase) of (a) Si- and (b) La-doped $HfO_2$ with 0%, 3.125%, and 6.25% doping concentrations. The section between the fifth and sixth points of 6.25% Si-doped $HfO_2$ (red box) was subdivided into 10 steps and is shown in part a (inset). The phase-transition routes were found by matching the direction of the $X_2'$ and $Y_5^z$ phonon modes, which survived in both the m- and o-phases. This was found to be the most favorable pathway with the lowest energy barrier. The 0%, 3.125%, and 6.25% cases are denoted as open, half-filled, and fully filled squares. The very large structural deformations and similarities between the m- and o-phases in Si-doped $HfO_2$ are expressed with red (for the m-phase) and green (for the o-phase) arrows.

S12) were scaled with respect to the original pathway (L) of undoped $HfO_2$.

Parts a and b of Figure 4 show the changes in the phase-transition energy from the m-phase to the o-phase induced by Si and La doping. In the case of Si, as the doping concentration increased, the ambiguities in the phase boundary between the m- and o-phases became prominent, shortening the corresponding *x*-axis length. In addition, the energy barrier (from o-phase to the m-phase) decreased from 44.55 meV $f.u.^{-1}$ in the undoped case (o → m) to 13.86 meV $f.u.^{-1}$ (o″ → m″) with the 3.125% concentration and 0 meV $f.u.^{-1}$ (o′ → m′) with the 6.25% concentration, reductions of 68.89% and 100%, respectively. We recognized that the vanished energy barrier for phase transition between the m- and o-phases could create confusion such as no longer a local minimum state of the o-phase or the potential of immediate transformation from the o-phase to the m-phase. To confirm our calculations, we subdivided the fifth and sixth points of the 6.25% Si-doped graph, which is marked with a red box, into 10 steps. The result of each point is shown in Figure 4a (inset). As shown in the inset, there was a clear barrier energy between the fifth and sixth points, indicating that the sixth point (o-phase) is the metastable phase and the immediate transformation from the o-phase to the m-phase will not occur. In contrast, in the case of La, despite an increasing doping concentration, the corresponding *x*-axis length hardly changed compared to the undoped case, and the energy barrier only slightly decreased from 44.55 meV $f.u.^{-1}$ in the undoped case to 35.99 meV $f.u.^{-1}$ with the 3.125% concentration (a 19.27% decrease) and 23.64 meV $f.u.^{-1}$ with the 6.25% concentration (a 46.94% decrease). At the 6.25% La doping concentration, there was a clear energy barrier compared to the case of Si, where the barrier disappeared completely.

In short, as the doping ratio increased, the relative o-phase stabilities induced by both Si and La were similar, whereas the activation energy (o′ → m′) of the Si-doped case disappeared and that of the La-doped case decreased but did not disappear. A 2018 report[21] has indicated that the wake-up slope, referring to the increased amount of polarization during a certain ferroelectric switching cycle, of undoped o-$HfO_2$ is approximately 0.4, and the slope at the concentration having the highest $P_r$ value is 0.16 for La (∼10 cat %) and 0.38 for Si (∼5 cat %). Even though the o-phase fraction at each doping concentration was the same at ∼80%, the wake-up slope was much greater in Si-doped $HfO_2$ than in La-doped $HfO_2$. These observations were consistent with our calculations in that the structural similarities between the m- and o-phases driven by Si doping increased and weakened the phase boundary between the two.

## 4. CONCLUSION

In summary, we identified the superior ability of Si and La dopants to stabilize o-phase $HfO_2$ by comparing the relative energies of the ground-state m-phase and ferroelectric o-phase. We also revealed the effects of these two dopants on the wake-up effect in $HfO_2$. First, we found that the greater the difference between the ionic radii of Hf and the dopant, the greater the relative stability of the o-phase compared to the m-phase; therefore, Si and La exhibited the most noticeable effects. Second, through phonon-mode analysis, we identified that structural deformation induced by Si doping produced structural components in the o-phase that were similar to those of the ground state (m-phase), whereas La did not have this effect. This isosymmetric effect reduced the structural differences between the m- and o-phases, as manifested in a strong local shear strain in the o-phase and confirmed by STEM analysis of an experimental thin film. The activation energy from the m-phase to the o-phase was also expected to be significantly lowered by Si, thereby facilitating the ferroelectric phase transition and suggesting an effective tuning strategy for the undesirable "wake-up" effect. However, for the La dopant, this stabilization mechanism was not clearly revealed compared with Si. So, we hope a further study of La-doped o-phase stabilization could be dealt with as future work.

## ■ ASSOCIATED CONTENT

### Supporting Information

The Supporting Information is available free of charge at https://pubs.acs.org/doi/10.1021/acs.inorgchem.9b03785.

Calculation method, methodology of phonon-mode displacement analysis and analytical data, structural and electronic studies, additional STEM data, and methodology of scaled pathways of transition (PDF)



https://dx.doi.org/10.1021/acs.inorgchem.9b03785
*Inorg. Chem.* 2020, 59, 5993−5999

## AUTHOR INFORMATION


### Corresponding Authors

**Jungwon Park** – *School of Chemical and Biological Engineering, Institute of Chemical Processes, Seoul National University, Seoul 08826, Republic of Korea; Center for Nanoparticle Research, Institute for Basic Science, Seoul 08826, Republic of Korea;* orcid.org/0000-0003-2927-4331; Email: jungwonpark@snu.ac.kr

**Jun Hee Lee** – *School of Energy and Chemical Engineering, Ulsan National Institute of Science and Technology, Ulsan 44919, Republic of Korea;* orcid.org/0000-0001-5121-244X; Email: junhee@unist.ac.kr

### Authors

**Hyemi Yang** – *School of Energy and Chemical Engineering, Ulsan National Institute of Science and Technology, Ulsan 44919, Republic of Korea*

**Kunwoo Park** – *School of Chemical and Biological Engineering, Institute of Chemical Processes, Seoul National University, Seoul 08826, Republic of Korea; Center for Nanoparticle Research, Institute for Basic Science, Seoul 08826, Republic of Korea*

**Hyun-Jae Lee** – *School of Energy and Chemical Engineering, Ulsan National Institute of Science and Technology, Ulsan 44919, Republic of Korea*

**Jinhyeong Jo** – *School of Energy and Chemical Engineering, Ulsan National Institute of Science and Technology, Ulsan 44919, Republic of Korea*

**Hayoung Park** – *School of Chemical and Biological Engineering, Institute of Chemical Processes, Seoul National University, Seoul 08826, Republic of Korea; Center for Nanoparticle Research, Institute for Basic Science, Seoul 08826, Republic of Korea*

**Noejung Park** – *Department of Physics, Ulsan National Institute of Science and Technology, Ulsan 44919, Republic of Korea;* orcid.org/0000-0002-2359-0635

Complete contact information is available at:
https://pubs.acs.org/10.1021/acs.inorgchem.9b03785


### Author Contributions

[†]The manuscript was written through contributions of all authors. All authors have given approval to the final version of the manuscript. These authors contributed equally.

### Notes

The authors declare no competing financial interest.

## ACKNOWLEDGMENTS

Financial support from the Creative Materials Discovery (Grant 2017M3D1A1040828), Basic Science Research (Grant 2017R1D1A1B03028004), Basic Research Laboratory (Grant NRF2017R1A4A1015323), Ministry of Trade, Industry Energy (Grant 10080657), and Korea Semiconductor Research Consortium programs and U−K Brand (1.200030.01) of UNIST support programs are gratefully acknowledged. K.P, H.P, and J.P. acknowledge Institutes for Basic Science (IBS-R006-D1) and the National Research Foundation of Korea (NRF) grant funded by the Korea government (MSIT) (No. NRF-2017R1A5A1015365). We also appreciate the supercomputing resources, including technical support, supplied by the Supercomputing Center/Korea Institute of Science and Technology Information (Grant KSC-2017-C3-0018).

## REFERENCES


(1) Wilk, G. D.; Wallace, R. M.; Anthony, J. M. High-k gate dielectrics: Current status and materials properties considerations. *J. Appl. Phys.* **2001**, *89*, 5243.

(2) Maiti, C. K.; Maikap, S.; Chatterjee, S.; Nandi, S. K.; Samanta, S. K. Hafnium oxide gate dielectric for strained-Si1xGex. *Solid-State Electron.* **2003**, *47* (11), 1995−2000.

(3) Böscke, T.; Müller, J.; Bräuhaus, D.; Schröder, U.; Böttger, U. Ferroelectricity in hafnium oxide thin films. *Appl. Phys. Lett.* **2011**, *99* (10), 102903.

(4) Long, S.; Lian, X.; Cagli, C.; Cartoixa, X.; Rurali, R.; Miranda, E.; Jiménez, D.; Perniola, L.; Liu, M.; Suñé, J. Quantum-size effects in hafnium-oxide resistive switching. *Appl. Phys. Lett.* **2013**, *102* (18), 183505.

(5) Schroeder, U.; Yurchuk, E.; Müller, J.; Martin, D.; Schenk, T.; Polakowski, P.; Adelmann, C.; Popovici, M. I.; Kalinin, S. V.; Mikolajick, T. Impact of different dopants on the switching properties of ferroelectric hafniumoxide. *Jpn. J. Appl. Phys.* **2014**, *53* (8S1), 08LE02.

(6) Starschich, S.; Boettger, U. An extensive study of the influence of dopants on the ferroelectric properties of $HfO_2$. *J. Mater. Chem. C* **2017**, *5* (2), 333−338.

(7) Hyuk Park, M.; Joon Kim, H.; Jin Kim, Y.; Moon, T.; Seong Hwang, C. The effects of crystallographic orientation and strain of thin $Hf_{0.5}Zr_{0.5}O_2$ film on its ferroelectricity. *Appl. Phys. Lett.* **2014**, *104* (7), 072901.

(8) Materlik, R.; Künneth, C.; Kersch, A. The origin of ferroelectricity in $Hf_{1-x}Zr_xO_2$: A computational investigation and a surface energy model. *J. Appl. Phys.* **2015**, *117* (13), 134109.

(9) Shandalov, M.; McIntyre, P. C. Size-dependent polymorphism in $HfO_2$ nanotubes and nanoscale thin films. *J. Appl. Phys.* **2009**, *106* (8), 084322.

(10) Böscke, T.; Teichert, S.; Bräuhaus, D.; Müller, J.; Schröder, U.; Böttger, U.; Mikolajick, T. Phase transitions in ferroelectric silicon doped hafnium oxide. *Appl. Phys. Lett.* **2011**, *99* (11), 112904.

(11) Müller, J.; Schröder, U.; Böscke, T.; Müller, I.; Böttger, U.; Wilde, L.; Sundqvist, J.; Lemberger, M.; Kücher, P.; Mikolajick, T.; Frey, L. Ferroelectricity in yttrium-doped hafnium oxide. *J. Appl. Phys.* **2011**, *110* (11), 114113.

(12) Mueller, S.; Mueller, J.; Singh, A.; Riedel, S.; Sundqvist, J.; Schroeder, U.; Mikolajick, T. Incipient ferroelectricity in Al-doped $HfO_2$ thin films. *Adv. Funct. Mater.* **2012**, *22* (11), 2412−2417.

(13) Mueller, S.; Adelmann, C.; Singh, A.; Van Elshocht, S.; Schroeder, U.; Mikolajick, T. Ferroelectricity in Gd-doped $HfO_2$ thin films. *ECS J. Solid State Sci. Technol.* **2012**, *1* (6), N123−N126.

(14) Lomenzo, P. D.; Zhao, P.; Takmeel, Q.; Moghaddam, S.; Nishida, T.; Nelson, M.; Fancher, C. M.; Grimley, E. D.; Sang, X.; LeBeau, J. M.; Jones, J. L. Ferroelectric phenomena in Si-doped $HfO_2$ thin films with TiN and Ir electrodes. *J. Vac. Sci. Technol., B: Nanotechnol. Microelectron.: Mater., Process., Meas., Phenom.* **2014**, *32* (3), 03D123.

(15) Hyuk Park, M.; Joon Kim, H.; Jin Kim, Y.; Lee, W.; Moon, T.; Seong Hwang, C. Evolution of phases and ferroelectric properties of thin $Hf_{0.5}Zr_{0.5}O_2$ films according to the thickness and annealing temperature. *Appl. Phys. Lett.* **2013**, *102* (24), 242905.

(16) Lee, T. Y.; Lee, K.; Lim, H. H.; Song, M. S.; Yang, S. M.; Yoo, H. K.; Suh, D. I.; Zhu, Z.; Yoon, A.; MacDonald, M. R.; Lei, X.; Jeong, H. Y.; Lee, D.; Park, K.; Park, J.; Chae, S. C. Ferroelectric Polarization-Switching Dynamics and Wake-Up Effect in Si-Doped $HfO_2$. *ACS Appl. Mater. Interfaces* **2019**, *11* (3), 3142−3149.

(17) Grimley, E. D.; Schenk, T.; Mikolajick, T.; Schroeder, U.; LeBeau, J. M. Atomic Structure of Domain and Interphase Boundaries in Ferroelectric $HfO_2$. *Adv. Mater. Interfaces* **2018**, *5*, 1701258.

(18) Xu, L.; Nishimura, T.; Shibayama, S.; Yajima, T.; Migita, S.; Toriumi, A. Kinetic pathway of the ferroelectric phase formation in doped $HfO_2$ films. *J. Appl. Phys.* **2017**, *122* (12), 124104.

(19) Pešić, M.; Fengler, F. P. G.; Larcher, L.; Padovani, A.; Schenk, T.; Grimley, E. D.; Sang, X.; LeBeau, J. M.; Slesazeck, S.; Schroeder, U.; Mikolajick, T. Physical mechanisms behind the field-cycling

behavior of $HfO_2$-based ferroelectric capacitors. *Adv. Funct. Mater.* **2016**, *26* (25), 4601−4612.

(20) Starschich, S.; Griesche, D.; Schneller, T.; Böttger, U. Chemical solution deposition of ferroelectric hafnium oxide for future lead free ferroelectric devices. *ECS J. Solid State Sci. Technol.* **2015**, *4* (12), P419−P423.

(21) Schroeder, U.; Richter, C.; Park, M. H.; Schenk, T.; Pešic, M.; Hoffmann, M.; Fengler, F. P.; Pohl, D.; Rellinghaus, B.; Zhou, C.; Chung, C.-C; Jones, J. L.; Mikolajick, T. Lanthanum-doped hafnium oxide: a robust ferroelectric material. *Inorg. Chem.* **2018**, *57* (5), 2752−2765.

(22) Lee, C.-K.; Cho, E.; Lee, H.-S.; Hwang, C. S.; Han, S. First-principles study on doping and phase stability of $HfO_2$. *Phys. Rev. B: Condens. Matter Mater. Phys.* **2008**, *78* (1), 012102.

(23) Künneth, C.; Materlik, R.; Falkowski, M.; Kersch, A. Impact of four-valent doping on the crystallographic phase formation for ferroelectric $HfO_2$ from first-principles: implications for ferroelectric memory and energy-related applications. *ACS Applied Nano Materials* **2018**, *1* (1), 254−264.

(24) Schenk, T.; Mueller, S.; Schroeder, U.; Materlik, R.; Kersch, A.; Popovici, M.; Adelmann, C.; Van Elshocht, S.; Mikolajick, T. Strontium doped hafnium oxide thin films: Wide process window for ferroelectric memories. *2013 Proceedings of the European Solid-State Device Research Conference (ESSDERC)*, Sept 16−20, 2013, Bucharest, Romania; IEEE, 2013; pp 260−263.

(25) Falkowski, M.; Künneth, C.; Materlik, R.; Kersch, A. Unexpectedly large energy variations from dopant interactions in ferroelectric $HfO_2$ from high-throughput ab initio calculations. *npj Computational Materials* **2018**, *4* (1), 73.

(26) Batra, R.; Huan, T. D.; Rossetti, G. A., Jr; Ramprasad, R. Dopants promoting ferroelectricity in Hafnia: Insights from A comprehensive chemical space exploration. *Chem. Mater.* **2017**, *29* (21), 9102−9109.

(27) Materlik, R.; Künneth, C.; Mikolajick, T.; Kersch, A. The impact of charge compensated and uncompensated strontium defects on the stabilization of the ferroelectric phase in $HfO_2$. *Appl. Phys. Lett.* **2017**, *111* (8), 082902.

(28) Materlik, R.; Künneth, C.; Falkowski, M.; Mikolajick, T.; Kersch, A. Al-, Y-, and La-doping effects favoring intrinsic and field induced ferroelectricity in $HfO_2$: A first principles study. *J. Appl. Phys.* **2018**, *123* (16), 164101.

(29) Zhou, D.; Xu, J.; Li, Q.; Guan, Y.; Cao, F.; Dong, X.; Müller, J.; Schenk, T.; Schröder, U. Wake-up effects in Si-doped hafnium oxide ferroelectric thin films. *Appl. Phys. Lett.* **2013**, *103*, 192904.

(30) Starschich, S.; Menzel, S.; Böttger, U. Evidence for oxygen vacancies movement during wake-up in ferroelectric hafnium oxide. *Appl. Phys. Lett.* **2016**, *108*, 032903.

(31) Shibayama, S.; Xu, L.; Migita, S.; Toriumi, A. Study of wake-up and fatigue properties in doped and undoped ferroelectric $HfO_2$ in conjunction with piezo-response force microscopy analysis. *2016 IEEE Symposium on VLSI Technology*, June 15−17, 2016, Honolulu, HI; IEEE, 2016, pp 1 and 2.

(32) Reyes-Lillo, S. E.; Garrity, K. F.; Rabe, K. M. Antiferroelectricity in thin-film $ZrO_2$ from first principles. *Phys. Rev. B: Condens. Matter Mater. Phys.* **2014**, *90* (14), 140103.



https://dx.doi.org/10.1021/acs.inorgchem.9b03785
*Inorg. Chem.* 2020, 59, 5993−5999